# Observed radar reflectivity in convectively coupled Kelvin and mixed Rossby-gravity waves

A. Swann,[1] A. H. Sobel,[2] S. E. Yuter,[3] and G. N. Kiladis[4]

Received 7 February 2006; revised 20 March 2006; accepted 18 April 2006; published 20 May 2006.

[1] Propagating disturbances in the tropical atmosphere exhibiting characteristics of linear equatorial waves have been shown to be ''coupled'' to convection. In some cases, a rain event at a specific location can be associated with a particular wave of sufficiently large amplitude. Rain events spanning three years at Kwajalein Atoll, Republic of the Marshall Islands, 8.72°N 167.73°E, are classified by associated wave type (i.e. Kelvin or mixed Rossby-gravity (MRG)) using space-time spectral-filtered outgoing longwave radiation (OLR). Contoured frequency by altitude diagrams (CFADs) of radar for the classified dates were compared between the two groups. The Kelvin wave accumulated CFAD has a distribution shifted to lower reflectivities compared to MRG suggesting that Kelvin storms likely contain a larger fraction of stratiform to convective area compared to MRG storms.
**Citation:** Swann, A., A. H. Sobel, S. E. Yuter, and G. N. Kiladis (2006), Observed radar reflectivity in convectively coupled Kelvin and mixed Rossby-gravity waves, *Geophys. Res. Lett.*, *33*, L10804, doi:10.1029/2006GL025979.

## 1. Introduction

[2] Convectively coupled waves are large-scale tropical disturbances associated with deep convection which have dispersion properties predicted by dry linear equatorial wave theory. The deep convection associated with a particular type of convectively coupled wave is detectable by its distinct signature in the frequency-wavenumber spectrum of observed outgoing longwave radiation (OLR) [*Wheeler and Kiladis*, 1999]. In some cases, specific convectively coupled wave types can be associated with specific storm events at a particular location [*Straub and Kiladis*, 2002; *Sobel et al.*, 2004]. Here, we examine whether convective systems associated with two wave types may be different from one another in some way that is detectable from their statistical distributions of volumetric radar reflectivities. Our approach has some similarities to that of *Petersen et al.* [2003] who examined differences between convective systems occurring in different phases of the same wave type, but we look instead at differences across wave types. The results may present clues as to how the large-scale environment influences deep convection, which is the essence of the convective parameterization problem.

## 2. Data

[3] We use volumetric radar data from the scanning S-band Doppler radar on Kwajalein Island, Republic of the Marshall Islands, 8.72°N 167.73°E [*Houze et al.*, 2004; *Yuter et al.*, 2005]. The radar data were quality-controlled to remove non-meteorological echo and echoes within 157 km range from the radar were interpolated to a Cartesian grid with 2 km grid spacing in both the horizontal and vertical in the horizontal and vertical. The time series of near surface echo area >20 dBZ is used to estimate the area of precipitation that would be measurable from surface gauges (>0.5 mm/hr). Additionally, the area of radar echo at each height was tabulated for each radar volume. The joint probability distribution of reflectivity with height, referred to as a contoured frequency by altitude diagram [*Yuter and Houze*, 1995, CFAD], is used to characterize the statistical properties of the ensemble of radar echoes occurring in association with each wave type. The CFAD distills the observed three-dimensional radar reflectivity into a format that facilitates comparison of the bulk microphysical properties between groups of storms. At each height, the CFAD consists of a normalized probability density function (PDF) of radar echo intensity at that level. Our analysis uses radar scans made approximately every 6 minutes over the rainy season (July–December) for the four years 1999–2002.

[4] OLR data from NOAA polar-orbiting satellites [*Liebmann and Smith*, 1996] are used to identify large-scale propagating disturbances and to classify rain events as being associated with particular wave types. *Wheeler and Kiladis* [1999] (hereinafter referred to as WK99) describe a space-time spectral analysis using these OLR data. In the space-time domain they remove a red noise background spectrum, and find zonally propagating waves on synoptic to intraseasonal time scales. Figure 1 from *Straub and Kiladis* [2002] shows wave filtering using windows prescribed for Kelvin waves and Figure 3 from WK99 shows the same but for MRG waves. The method used to create wave-associated OLR for this analysis follows these studies, differing from WK99 only in that the total OLR, not just the symmetric component, is filtered and partitioned. This alternate method better captures the structure of the waves about the equator.

[5] Statistical composite maps (Figures 1 and 2) of wave events were made using anomalous OLR, filtered to remove periods longer than 30 days, and similarly filtered 850 mb

[1]Department of Earth and Planetary Science, University of California, Berkeley, California, USA.
[2]Department of Applied Physics and Applied Mathematics and Department of Earth and Environmental Sciences, Columbia University, New York, New York, USA.
[3]Department of Marine, Earth, and Atmospheric Sciences, North Carolina State University, Raleigh, North Carolina, USA.
[4]NOAA/Earth System Research Laboratory, Boulder, Colorado, USA.


0094-8276/06/2006GL025979$05.00

wind fields. Wind fields come from the NCEP-NCAR Reanalysis [*Kalnay et al.*, 1996].

## 3. Methods

### 3.1. Classification of Rain Events

[6] Rain events at Kwajalein were identified and classified into one of three categories–Kelvin, MRG, and other–using the following algorithm. OLR data filtered to retain only the Kelvin or MRG signal were reduced to time series by averaging over a region around Kwajalein from 165°–170°W and 0°–15°N. Smoothed amplitude time series were created by squaring these wave time series and applying a running mean. The length of the running mean window was chosen to be proportional to the lowest frequency retained for each wave type, and was 1.5 days for Kelvin, and 5.5 days for MRG.

[7] Event "matches" were chosen as times when both the echo area and wave amplitude series were each above two standard deviations from the time means over the data record. The resulting number of event "matches" was not sensitive to small changes in the criteria.

### 3.2. Composite Spatial Fields

[8] To test the validity of our classification of wave events, we created composite maps of low-level wind and total OLR anomaly (both filtered to remove periods longer than 30*d*) for each wave type. The three-year rain record at Kwajalein was reduced to 184 total event days broken down into categories of 52 Kelvin days, 48 MRG days, and 84 "other" days. The identified events from the Kelvin and MRG categories were used to create composite spatial maps of the 850 hPa winds and OLR during each storm. For each storm event, the day with a local minimum in wave-filtered

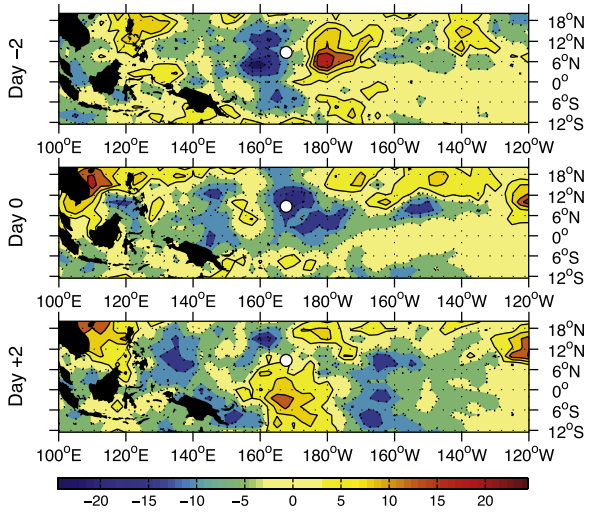


**Figure 1.** Composite map of anomalous OLR for Kelvin wave-associated storms. (middle) A composite of spatial variables on the storm day designated as "day 0", and (top and bottom) composites for two days preceding and following "day 0". Negative OLR values are shaded with dotted contour intervals of 3.4 $Wm^{-2}$ and positive OLR values contoured with solid lines at the same interval and a maximum of 27.1 $Wm^{-2}$. The location of Kwajalein is identified by a white dot.

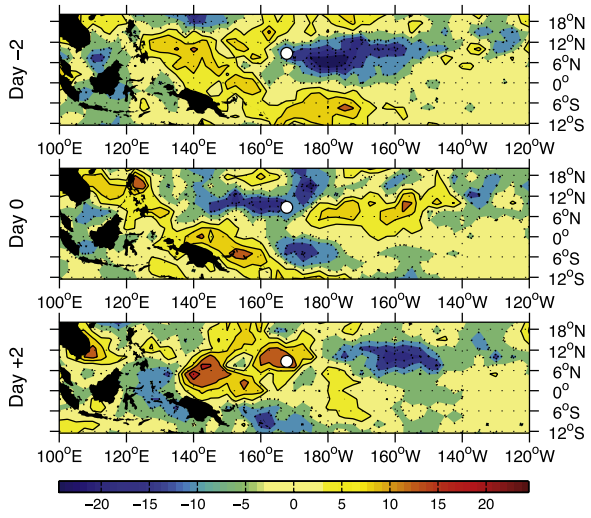


**Figure 2.** Same as Figure 1 but for MRG wave-associated storms using contour intervals of 3.5 $Wm^{-2}$ and a maximum of 23.3 $Wm^{-2}$.

OLR was chosen as "day 0" at Kwajalein. The spatial fields from day 0 from all events, as well as two days before and after, were averaged together to make the composite maps. Choosing the day with the minimum in wave OLR helps to align the phase of the storms so that shared features persist in the mean. Figures 1 and 2 show the anomalous OLR for Kelvin and MRG storms over a 5-day span surrounding the chosen day and Figures S1 and S2 (see auxiliary material[1]) show both the OLR and anomalous winds. We expect to see the fundamental wave patterns derived from the linear shallow water theory as given by *Matsuno* [1966] shown by *Wheeler et al.* [2000, Figures 6 and 14] (derived from *Matsuno* [1966]). In Figures 1 and 2, the OLR clearly shows propagation past Kwajalein with the Kelvin composite propagating eastward and the MRG composite propagating westward, as expected from theory. The wind patterns (see auxiliary material) do not conform tightly to the expected theoretical patterns in the spatial maps, but do show, for example, strong zonal winds to the East of the OLR maximum in the Kelvin, and much less zonal wind and more meridional wind, with vortical circulations centered approximately on the equator, in the MRG.

[9] The winds are further illustrated by Hovmoeller diagrams (Figures 3 and 4) of zonal winds for the Kelvin wave-associated storms and meridional winds for the MRG-associated storms. In the Kelvin case (Figure 3) a convergence in zonal wind is centered at day −1 near Kwajalein and the pattern propagates eastward, intensifying at day +1. In the MRG case (Figure 4) strong northerlies are centered to the east of Kwajalein near 175°W at day 0 and propagation is westward, as expected.

### 3.3. Composite CFADs

[10] Composite CFADs were made for each wave category by averaging at each point in height-reflectivity space all available CFADS in the category. The Kelvin category

[1] Auxiliary material is available in the HTML.

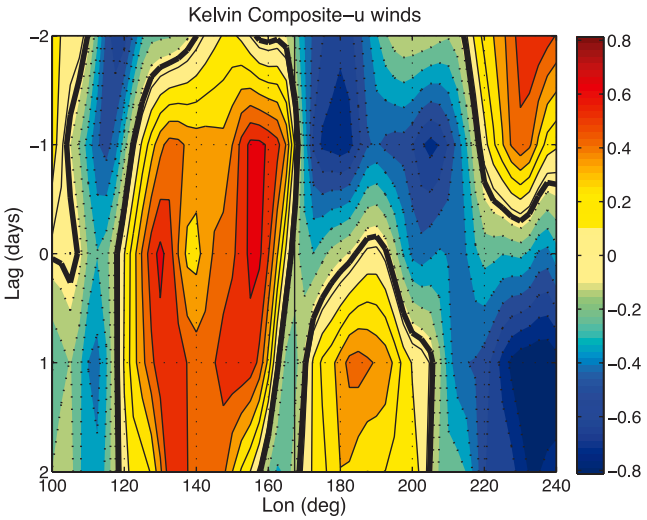


**Figure 3.** Composite Hovmoeller diagram of zonal wind (filtered to remove periods greater than 30*d* and averaged from 0 to 15N) for Kelvin wave-associated storms. Negative wind directions are shaded with dotted contour lines and positive wind anomalies are contoured with solid lines. The time axis is as in Figure 1 and the longitude of Kwajalein is identified by a black line.

CFADs consisted of data from 52 days and the MRG from 48 days. The mean CFADs for each group and the significant difference between them can be seen in Figure 5. We use a Monte Carlo simulation to test the significance. Using all Kelvin and MRG event days as a pool (totaling 100 event days), groups with equivalent numbers of days to the Kelvin and MRG groups were drawn randomly, averaged and differenced 1000 times. Our sample difference was considered significant when its absolute value exceeded that of 950 of the 1000 trial differences (95% significance). Only significant values are plotted in Figure 5c. The mean Kelvin CFAD shows a small shift of the distribution mode to smaller reflectivity values compared to the mean MRG at all heights. MRG storms have a wider distribution of reflectivity in the ice layer and a rain layer reflectivity distribution skewed to higher values compared to Kelvin. The result in Figure 5c was tested for seasonal bias by weighting CFADs equally by month. Mean CFADs for each category were computed separately for each month of the year, including all cases occurring in that month, and these were averaged together to produce one averaged CFAD for each category. No significant difference in the results was found between this method and the one described above. A second normalization scheme was also tested which weights the data from any particular day equally by taking the mean of each day in a group separately before taking the mean of the whole group. This method gives very similar results to the first method described above which weights every CFAD measurement (taken approximately every 6 minutes) equally. Additionally, the mean sea surface temperature surrounding Kwajalein was not significantly different between the Kelvin and MRG samples.

[11] Other statistics were also computed to compare the two groups. Confidence limits were computed by Monte Carlo simulation as described above. The daily mean OLR anomaly was more negative for Kelvin storms than MRG storms (at 95% significance), but the distribution of echo area sizes were statistically similar between groups. Nonetheless, the difference in the CFAD mode between groups suggests relatively more convective precipitation area (less stratiform precipitation area) in MRG storms compared to Kelvin storms. Since degree of mesoscale organization is related to stratiform relative area, this in turn implies that Kelvin storms may have more developed mesoscale circulations compared to MRG storms. Future work will attempt to determine the relation between mesoscale organization and storm intensity by partitioning the precipitation explicitly into convective and stratiform components.

## 4. Conclusions

[12] All major rain events (rainfall >2 standard deviations from the mean) at Kwajalein were classified into one of three groups associated with large-scale wave dynamics, Kelvin, MRG, and "other". Rain events were assigned to these categories by finding coincident large anomalies of the appropriate signs in both the smoothed amplitude filtered OLR time series for the wave in question and the time series of surface 20 dBZ radar echo area. The CFADs were composited based on the wave-associated storm dates; then, the Kelvin and MRG groups were compared by taking the difference of the mean CFAD for each group. These mean CFADs show detectable differences according to wave type, with the mode of the Kelvin CFAD shifted to lower reflectivities compared to MRG. This suggests that MRG storms may have more convective precipitation area relative to total storm area compared to Kelvin storms.

[13] At present, this is purely an observational result, for which we do not have an explanation. We can think of various ways in which waves alter the large-scale environment in which deep cumulus convection occurs. For example, waves induce vertical motion, which can alter the temperature and humidity profiles; alter surface winds (and thus surface fluxes); and advect moisture. Different wave types presumably act, via these various mechanisms, in different ways, leading to differences in mesoscale

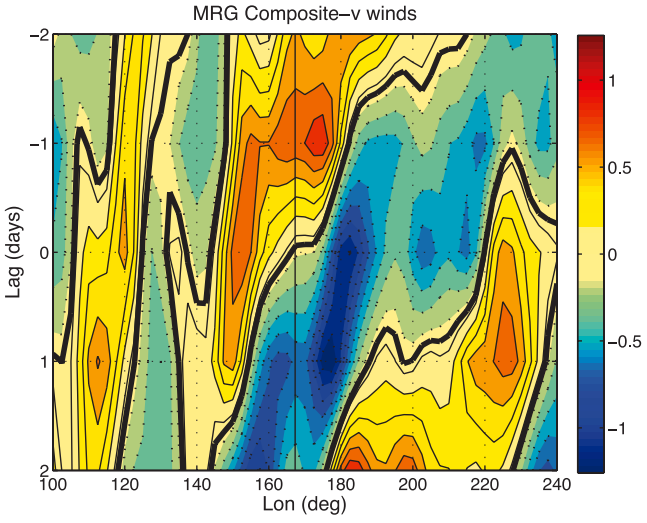


**Figure 4.** Same as Figure 3 but for meridional winds for MRG wave-associated storms.

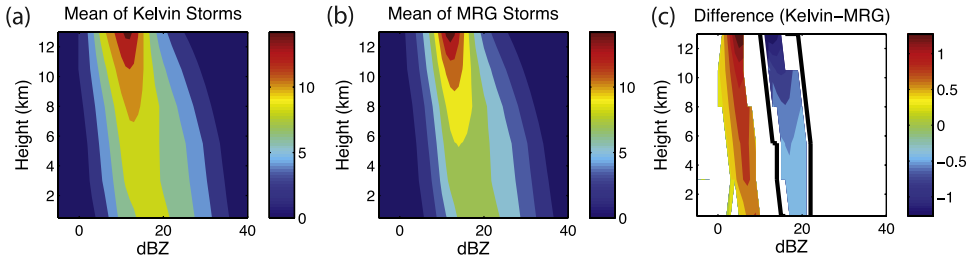


**Figure 5.** (a and b) The mean CFADs of reflectivity for Kelvin and MRG wave-associated storm days. (c) The significant difference between Figures 5a and 5b as determined by Monte Carlo simulation. Despite falling outside the significant region, the contour interval for zero has been drawn with a think black line to highlight the negative and positive regions. Each CFAD consists of a PDF of reflectivity at each height multiplied by 100 so that values are in percent.

convective dynamics which manifest themselves in our results. For example, a wave which propagates faster, relative to the mean flow, will have less time to interact with the surrounding air mass compared to one which propagates slower. A slower wave will have more time to modify the air mass in which it is travelling, potentially allowing humidity feedbacks to be more effective [*Sobel and Horinouchi*, 2000]. Whether this or some other difference in large-scale wave forcing is responsible for the differences in convection which we observe, and how those forcing differences lead to the convection differences, is a matter for future research.

[14] **Acknowledgments.** This work was supported by NASA grants NNG04GA73G and NNG04GA65G, and by an NSF IGERT fellowship to A. Swann at Columbia University. We would like to thank Catherine Spooner and Timothy Downing for their help with data acquisition and radar data processing respectively, Cristina Perez for her comments and assistance editing, and Mark Cane, Anthony Del Genio and Brian Mapes for discussions. This work was completed primarily while the first author was a student at Columbia University.

## References

Houze, R. A., et al. (2004), Uncertainties in oceanic radar rain maps at Kwajalein and implications for satellite validation, *J. Appl. Meteorol.*, *43*, 1114–1132.

Kalnay, E., et al. (1996), The NCEP/NCAR 40-year reanalysis project, *Bull. Am. Meterol. Soc.*, *77*, 437–471.

Liebmann, B., and C. A. Smith (1996), Description of a complete (interpolated) outgoing longwave radiation dataset, *Bull. Am. Meterol. Soc.*, *77*, 1275–1277.

Matsuno, T. (1966), Quasi-geostrophic motions in the equatorial area, *J. Meteorol. Soc. Jpn.*, *44*, 25–43.

Petersen, W. A., et al. (2003), Convection and easterly wave structures observed in the eastern Pacific warm pool during EPIC-2001, *J. Atmos. Sci.*, *60*, 1754–1773.

Sobel, A. H., and T. Horinouchi (2000), On the dynamics of easterly waves, monsoon depressions, and tropical depression type disturbances, *J. Meteorol. Soc. Jpn.*, *78*, 167–173.

Sobel, A. H., et al. (2004), Large-scale meteorology and deep convection during TRMM KWAJEX, *Mon. Weather Rev.*, *132*, 422–444.

Straub, K. H., and G. N. Kiladis (2002), Observations of a convectively coupled Kelvin wave in the eastern Pacific ITCZ, *J. Atmos. Sci.*, *59*, 30–53.

Wheeler, M., and G. N. Kiladis (1999), Convectively coupled equatorial waves: Analysis of clouds and temperature in the wavenumber-frequency domain, *J. Atmos. Sci.*, *56*, 374–399.

Wheeler, M., et al. (2000), Large-scale dynamical fields associated with convectively coupled equatorial waves, *J. Atmos. Sci.*, *57*, 613–640.

Yuter, S. E., and R. A. Houze (1995), 3-Dimensional kinematic and microphysical evolution of Florida cumulonimbus: 2. Frequency-distributions of vertical velocity, reflectivity, and differential reflectivity, *Mon. Weather Rev.*, *123*, 1941–1963.

Yuter, S. E., et al. (2005), Physical characterization of tropical oceanic convection observed in KWAJEX, *J. Appl. Meteorol.*, *44*, 385–415.

G. N. Kiladis, NOAA/Earth System Research Laboratory, 325 Broadway, Boulder, CO 80305–3337, USA.

A. H. Sobel, Department of Applied Physics and Applied Mathematics, Columbia University, Room 217, 500 West 120th Street, New York, NY 10027, USA.

A. Swann, Department of Earth and Planetary Science, University of California, Berkeley, 307 McCone Hall #4767, Berkeley, CA 94720–4767, USA. (aswann@atmos.berkeley.edu)

S. E. Yuter, Department of Marine, Earth and Atmospheric Sciences, Campus Box 8208, North Carolina State University, Raleigh, NC 27695–8208, USA.